UCSF

UC San Francisco Previously Published Works

Title

Independent reaction times method in Geant4-DNA: Implementation and performance

Permalink

Journal

ISSN

Authors

Ramos-Méndez, José
Shin, Wook-Geun
Karamitros, Mathieu
et al.

Publication Date

DOI

Peer reviewed

Independent Reaction Times method in Geant4-DNA: implementation and performance.

José Ramos-Méndez[1,*], **Wook-Geun Shin**[2,3], **Mathieu Karamitros**[4], **Jorge Domínguez-Kondo**[5], **Ngoc Hoang Tran**[2], **Sebastien Incerti**[2], **Carmen Villagrasa**[6], **Yann Perrot**[6], **Václav Štěpán**[7], **Shogo Okada**[8], **Eduardo Moreno-Barbosa**[5], **Bruce Faddegon**[1]

[1]Department of Radiation Oncology, University of California San Francisco, San Francisco CA, 94115, USA

[2]Université de Bordeaux, CNRS/IN2P3, UMR5797, Centre d'Études Nucléaires de Bordeaux Gradignan, 33175 Gradignan, France

[3]Department of Radiation Convergence Engineering, Yonsei University, 26493 Wonju, Korea

[4]Radiation Laboratory, University of Notre Dame, Notre Dame, In 46556, U.S.A

[5]Facultad de Ciencias Físico Matemáticas, Benemérita Universidad Autónoma de Puebla, Puebla PUE, 72000 MEX

[6]IRSN, Institut de Radioprotection et de Sûreté Nucléaire, BP17, 92262 Fontenay-aux-Roses, France

[7]Department of Radiation Dosimetry, Nuclear Physics Institute of the CAS, Prague, Czech Republic

[8]KEK, 1-1, Oho, Tsukuba, Ibaraki 305-0801, Japan

Abstract

Purpose: The simulation of individual particle tracks and the chemical stage following water radiolysis in biological tissue is an effective means of improving our knowledge of the physico-chemical contribution to the biological effect of ionizing radiation. However, the step-by-step simulation of the reaction kinetics of radiolytic species is the most time-consuming task in Monte Carlo track-structure simulations, with long simulation times that are an impediment to research. In this work, we present the implementation of the independent reaction times (IRT) method in Geant4-DNA Monte Carlo toolkit to improve the computational efficiency of calculating G-values, defined as the number of chemical species created or lost per 100 eV of deposited energy.

Methods: The computational efficiency of IRT, as implemented, is compared to that from available Geant4-DNA step-by-step simulations for electrons, protons and alpha particles covering a wide range of linear energy transfer (LET). The accuracy of both methods is verified using published measured data from fast electron irradiations for $^\bullet$OH and e^-_{aq} for time-dependent G-

---

[*]1600 Divisadero Street Suite HM006, San Francisco, CA 94115, USA. Jose.RamosMendez@ucsf.edu.

values. For IRT, simulations in the presence of scavengers irradiated by cobalt-60 γ-ray and 2 MeV protons are compared with measured data for different scavenging capacities. In addition, a qualitative assessment comparing measured LET-dependent G-values with Geant4-DNA calculations in pure liquid water is presented.

Results: The IRT improved the computational efficiency by three orders of magnitude relative to step-by-step while differences in G-values by 3.9% at 1 μs were found. At 7 ps, $^{\bullet}$OH and e^{-}_{aq} yields calculated with IRT differed from recent published measured data by 5%±4% and 2%±4%, respectively. At 1 μs, differences were 9%±5% and 6%±7% for $^{\bullet}$OH and e^{-}_{aq}, respectively. Uncertainties are one standard deviation. Finally, G-values at different scavenging capacities and LET-dependent G-values reproduced the behavior of measurements for all radiation qualities.

Conclusion: The comprehensive validation of the Geant4-DNA capabilities to accurately simulate the chemistry following water radiolysis is an ongoing work. The implementation presented in this work is a necessary step to facilitate performing such a task.

1   Introduction.

Modeling the reaction kinetics of chemical species produced by radiolysis has important applications in radiobiology and medical physics. At the cellular level, this modeling complements the quantification of biological damage by accounting for the indirect contributions from the radiolytic species, extending the knowledge of the effects of ionizing radiation in biological tissue. Chemical reaction kinetics constitute a stochastic process that is in alignment with the capabilities of track-structure simulations using the Monte Carlo method. Together they encompass the physical and chemical processes of the interaction of ionizing radiation with biological tissue. Along the years, sophisticated Monte Carlo track-structure (MCTS) codes have been developed, including KURBUC [1], PARTRACK [2], RITRACKS [3], TRAX-chem [4], IONLYS-IRT [5], and Geant4-DNA [6–9]. In some cases, the codes have the capability to integrate geometry models, like DNA in the cell nucleus, allowing the sampling of clustered DNA strand-breaks, which are the input of DNA repair models [1,10–14]. Until recently, MCTS codes have been restricted to the laboratories where they were developed, and then, their use in biology or medical physics fields have been limited, averaging only a few publications annually, as shown in Figure 1.

More than 10 years have passed since the Geant4 Collaboration [15–17] released Geant4-DNA, today the first open-source and multithreaded MCTS code [6–9]. Since 2013, this open source toolkit provides models and tools to simulate the water radiolysis process, including the physical, pre-chemical, and chemical stages [18–20]. Geant4-DNA is under active development (e.g.,[9]). This work is being done in parallel with the development of TOPAS-nBio, a wrapper to the toolkit to facilitate track structure and chemistry simulation of complex geometries incorporating cell structures, including DNA[21]. The impact of Geant4-DNA in the medical physics field since its introduction continues to increase (Figure 1). The development of Geant4-DNA is an ongoing work that includes further refinement and validation of physical models, radiation chemistry models, geometry models, damage scoring algorithms and computational efficiency improvement methods.

It is well known that MCTS codes demand a high computational cost. The overload is intrinsic due to the calculation of each and every ionization along the track of charged particles through matter. In addition, the use of the step-by-step method (SBS) for the realization of chemical reactions between radiolysis products increases dramatically the computing time for the simulation of biological effects (>99% of the execution time for an alpha particle of 4 MeV/u simulated with Geant4-DNA). To mitigate this overload, at the physical stage the use of variance reduction techniques [22] and the combination of condensed-history and track-structure transport [23] have shown significant enhancement of the computational efficiency of Geant4-DNA applications. For the chemical stage, the independent reaction times (IRT) technique has been developed to reduce the computational burden of simulating the reaction kinetics of chemical species [24–26]. IRT has been implemented in several MCST codes, mainly for the calculation of time-dependent radiolytic yields [3,5,21,26–28]. Given its flexibility, the algorithm can also accommodate the reaction of DNA molecules with reactive chemical species which leads to the estimation of early DNA damage, as shown in plasmid models [29] or the cell nucleus [12]. The high efficiency of IRT relative to step-by-step, and its flexibility to simulate biological damage, make this method a powerful tool with potential benefits to the research community. However, the availability of IRT, like open source MCTS, has been limited. For these reasons, the Geant4 collaboration has started to work actively on the implementation of this method in the code, either in its original/traditional version, using synchronous algorithm adapted to the calculation of DNA damage (Tran et al, accepted in Medical Physics), and an extended version that considers behavior of chemical species at boundaries [30]. A collective effort is also performed for comparing all these variants in order to specify the limits and advantages of each of them, which strongly depend on the applications.

In this work, we present details of the implementation and characterization of the IRT method in Geant4-DNA. We report the computational efficiency compared to SBS simulations and accuracy compared to experimental radiolytic yields. The implementation will be publicly released in forthcoming Geant4 version 10.7 Beta.

2   Methods.

2.1   The Independent Reaction Times.

The IRT method was developed to simulate reaction times in the diffusion kinetics process, as part of the simulation of the diffusion and reaction of radiolytic species and their reactive products following water radiolysis. The high computational efficiency of IRT compared to the alternative SBS method is achieved by avoiding the burden of simulating the detailed trajectory of each diffusing chemical species. In counterpart, this approach has the drawback of losing the spatial information of each individual chemical species. Instead, an iterative process is performed that begins at radiolysis and completes after all reactive species have reacted or an upper time limit has been reached. Following the independent pairs approximation, the initial positions of all the diffusive species produced at the end of the pre-chemical stage are used to simulate the reaction times between reactive pairs using probability functions. These functions represent solutions to the diffusion equation from the theory of diffusion kinetics. All the reactive pairs along with their reaction times are

assembled into an array that is sorted out in an ascendant way according to reaction times. Subsequently, the realization of the reactions is performed by removing from the array each reactive pair, starting with the pair with the shortest reaction time, and inserting the reactive products, if any. Each time a product is created, the corresponding reaction times with the remaining species in the array are sampled and resorted in an ascendant way. The process is finished when all the possible combinations are exhausted or an upper time limit is achieved, typically the 10^{-7}-10^{-6} s, signaling the end of the chemical stage, when the spatial distribution of species are considered as homogeneous [31]. Reactions with background solutions can be simulated as pseudo-first-order reactions with the continuum approach, assuming they are uniformly distributed in the background. In the continuum approach, each reactive species reacts with the background following an exponential distribution probability given by $1 - \exp(-k[B]\,t)$, where k[B] is the scavenging capacity of the solution [26]. For the implementation, the reaction times are obtained as t = -log(U)/k[B], where U is a random number uniformly distributed between 0 and 1.

2.1.1 Reaction schemes.

The implementation presented in this work, extends the previous scheme for SBS simulations of Geant4-DNA [18,19] developed on top of totally diffusion-controlled reactions (when two chemical species recombine with each other immediately at encounter), by incorporating the IRT method including partially diffusion-controlled reactions (when two chemical species do not recombine immediately when they encounter, [32]). The scheme to simulate the reaction times is based on the formalism developed [25,33], and later presented elsewhere [3,5,26]. The reader is referred to these publications for the mathematical details. The main probability functions are summarized below.

For totally diffusion-controlled reactions, the reaction times are sampled using the inverse of the probability functions solved for time *t*, given by Equations 1 and 2 for reactions where at least one chemical specie is neutral, and between charged particles, respectively.

$$P_{\mathrm{I}}(t \mid r_0) = \frac{\sigma}{r_0}\mathrm{Erfc}\left(\frac{r_0 - \sigma}{\sqrt{4Dt}}\right) \tag{1}$$

and,

$$P_{\mathrm{III}}(t \mid r_0) = \frac{\sigma_{\mathrm{eff}}}{r_{\mathrm{eff}}}\mathrm{Erfc}\left(\frac{r_{\mathrm{eff}} - \sigma_{\mathrm{eff}}}{\sqrt{4Dt}}\right) \tag{2}$$

where r_0 is the initial separation between chemical species, σ is the reaction radius and D is the sum of the diffusion coefficients. For charged particles, r_{eff} and σ_{eff} are the effective separation distance and effective reaction radius, respectively. These values are scaled from the natural separation and reaction radius to consider a Coulomb potential and are related by the Onsager's radius r_c as follows

$$r_{\mathrm{eff}} = \frac{-r_c}{1 - \exp\left(r_c/r_0\right)}, \quad \text{and} \quad \sigma_{\mathrm{eff}} = \frac{-r_c}{1 - \exp\left(r_c/\sigma\right)} \tag{3}$$

For partially diffusion-controlled reactions, the probability functions are assigned to a random number U uniformly distributed between 0 and 1 (i.e. $P_{II}(r, t|r_0) = U$) and solved numerically to obtain the time, t. Equation 4 corresponds to reactions where at least one chemical species is neutral, rewritten in terms of the diffusion k_{diff} and activation k_{act} reaction rate coefficients for computational implementation.

$$P_{II}(t|r_0) = \frac{k_{act}}{k_{diff}r_0\alpha}\left[\text{Erfc}\left(\frac{r_0-\sigma}{\sqrt{4Dt}}\right) - W\left(\frac{r_0-\sigma}{\sqrt{4Dt}}, -\alpha\sqrt{4Dt}\right)\right] \tag{4}$$

where, $\alpha = -(k_{act} + 4\pi\sigma D)/(4\pi\sigma^2 D)$ with k_{act} the activation reaction rate coefficient and $W(x, y) = \exp(2xy + y^2)\text{Erfc}(x + y)$. Equation 5 corresponds to reactions between charged particles, rewritten in terms of k_{diff} and the observed reaction rate coefficient k_{obs}:

$$P_{IV}(t|r_0) = \frac{\sigma_{eff}\,k_{obs}}{r_{eff}k_{diff}}[\text{Erfc}(b) - W(b, a)] \tag{5}$$

where,

$$a = \frac{4\sigma^2\alpha'}{r_c^2}\sqrt{\frac{t}{D}}\sinh^2\left(\frac{r_c}{2\sigma}\right), \quad \text{and} \quad b = \frac{r_c}{4\sqrt{Dt}}[\coth\left(\frac{r_c}{2r}\right) - \coth\left(\frac{r_c}{2\sigma}\right)] \tag{6}$$

with α' given by,

$$\alpha' = \frac{k_{act}}{4\pi\sigma^2} + \frac{r_c D}{\sigma^2\left(1 - \exp(-r_c/\sigma)\right)} \tag{7}$$

2.1.2 Implementation in Geant4-DNA.—Geant4-DNA, an extension of the Geant4 toolkit, is an object-oriented simulation toolkit written in C++ for the simulation of the passage of particles through the matter, the subsequent radiolysis and the reaction kinetics of chemical species. The software provides the tools distributed in C++ classes[a] which include functionalities to build geometry models, specify particle sources, invoke physics process and chemistry process, scoring capabilities, etc. In this way, Geant4-DNA allows building sophisticated simulations for radiobiology research. Details of the architecture of Geant4 and Geant4-DNA can be found elsewhere [6–9,17–20,34]. Details of the implementation of IRT in Geant4-DNA are presented here.

Figure 2 shows the flowchart diagram of the implementation of IRT in Geant4-DNA developed in this work (version 10.7 beta, June 2020). The dissociation channels of the pre-chemical stage (Table A1) and the chemical reactions are declared and initialized in the chemistry class constructor[b] **G4EmDNAChemistry_option3**, which includes the list of molecular chemical species, chemical reactions and their type. The set of reactions implemented are those listed for the RITRACKS software elsewhere [3], see appendix A.

---

[a] A C++ class is a user-defined concrete representation of a concept (i.e. a type), designed to provide a new type that has no direct counterpart among the built-in C++ types.[67]
[b] A constructor is a function with the explicit purpose of initializing objects (i.e. construct) of a give type.[67]

Provisions are made within the class constructor to facilitate activating or deactivating individual reactions in Geant4-DNA applications. Parameters for the chemical reactions are pre-calculated in the **G4DNAMolecularReactionTable** class. By the end of pre-chemical stage, the initial chemical species are automatically stored in a vector defined in the **G4ITTrackHolder** class. From this class, a loop is performed to identify all possible reactive pairs from all the initial chemical species. Subsequently, reactions at contact are evaluated using equation 8 [3,5,35] which overcomes the cases when the interparticle distance is smaller than the effective reaction radius and hence the IRT method cannot be used, for example in equation 1 the probability is greater than one if $r_0 < \sigma$.

$$P_{\text{react}} = \frac{-\exp\left(-\frac{r_c}{\sigma + \varrho}\right)}{\exp\left(-\frac{r_c}{\sigma}\right) - \exp\left(-\frac{r_c}{\sigma + \varrho}\right) - \left(\frac{k_{\text{diff}}}{k_{\text{act}}}\right)\left(1 - \exp\left(-\frac{r_c}{\sigma}\right)\right)} \tag{8}$$

In equation 8, $\varrho = 0.29$ nm, the approximate distance between neighboring water molecules; and $P_{\text{react}} = 1$ for totally diffusion-controlled reactions ($k_{\text{act}} \rightarrow \infty$) as expected.

The identified remaining reactive pairs, defined internally as "reactions", are stored in the reaction list defined in the **G4ITReactionSet** class with their corresponding reaction time, called random reaction time (RRT in figure 2). The RRT values are sampled depending on the type of reaction using equations 1, 2, 4 and 5, whereas the adopted acceptance-rejection methods are described in detail elsewhere[3]. **G4ITReactionSet** uses an ordered multiset container to sort in ascending order the RRT values. Subsequently, one more loop is performed for the realization of reactions, that is, to remove from the reaction list the reactive pairs (named speciesA and speciesB in Figure 2), starting with the pairs having the shortest RRT value. All remaining "reactions" that include any of the reactive species involved are also removed. If chemical species are produced by the reaction, then all of the possible reactive pairs along with the remaining chemical species in **G4ITTrackHolder** are identified and inserted in the reaction list with the corresponding RRT value. The spatial positions of the products are calculated with the *position approach* described elsewhere[24]. Finally, the **G4MoleculeCounter** class counts the number of chemical species and calculates G-values (number of chemical species produced or lost per 100 eV of deposit energy) as a function of time.

To reduce the computational burden of searching reactive pairs separated by long distances, we limit the search range for a reactive chemical species among its neighbors based on a confidence level for reaction. To this end, the simulation medium is voxelized into cubic voxels of side length σ_{off} (Figure 3), the searching range described elsewhere [19]. The parameter σ_{off} was set to 550 nm, giving a 95% confidence level for the species with higher reaction rate (H_3O^+, table A2). Thus, for a given chemical species, shown with a yellow star in Figure 3, all the possible reactions are searched within the 27 voxels around it (in 3-dimensions).

To incorporate the IRT method within the chemistry framework of Geant4-DNA, new classes have been developed among the Geant4 kernel classes. In this way, the users can

easily swap between the SBS method or the IRT method in any physics list (e.g. selecting **G4EmDNAChemistry_option3** for IRT or **G4EmDNAChemistry up to option 2** for SBS), taking advantage of the features previously developed for the SBS method, described elsewhere [18,19].

2.2 Verification.

2.2.1 Physical models and water dissociation scheme.

The simulation of the physical stage is done on a history-by-history basis, starting with a source particle traversing the geometry, ionizing atoms in its wake, followed by water radiolysis with diffusion and reaction of the reactive chemical species. For the simulation of physical interactions in liquid water (e.g. electronic excitation, ionization, elastic scattering, etc.), Geant4-DNA adopts a discrete approach ("track structure") in which all interactions are explicitly simulated, without the use of cuts for the control of the production of secondary particles. Such an approach ensures a better accuracy, particularly adapted to low energy (< 100 eV) and small dimension (< micrometer) particle tracking [36]. Geant4-DNA provides different sets of models for the simulation of physical interactions, assembled in "physics constructors" which assign each particle type to a list of physical interactions they can undergo along with the corresponding models needed to simulate such interaction. We previously described in detail the three alternative constructors currently available in Geant4-DNA, differing only by the theoretical approaches they adopt for the description of electron interactions and by their energy range coverage [9]

For this study, we selected the "G4EmDNAPhysics_option2" physics constructor, which provides the largest energy coverage for electrons in Geant4-DNA (7.4 eV to 1 MeV). In brief, this constructor describes the interactions of electrons, photons, protons, neutral hydrogen, alpha particles and their charged states and heavier ions (^{7}Li, ^{9}Be, ^{11}B, ^{12}C, ^{14}N, ^{16}O, ^{28}Si and ^{56}Fe). Regarding electron interactions, this constructor describes inelastic processes based on the formalism of the complex dielectric response function of liquid water, considering four ionization shells and five discrete electronic excitation states [37]. Ionization of the K-shell is calculated from the Binary-Encounter-Approximation-with-Exchange model [38]. Regarding the modeling of elastic scattering for electrons, for this work we have replaced the default model based on the partial wave theory by a newly developed model calculated using the ELSEPA code [39,40]. Regarding the thermalization distance of sub-excited electrons, the model adopted is derived from Monte Carlo simulations using cross-sections of Michaud et al [41] for amorphous ice, scaled by Meesungnoen et al [42] to consider the difference between amorphous and liquid-phase water. The model is applied with an upper energy limit of 7.4 eV. In the case of electrons induced by auto-ionization of excited water molecules at the pre-chemical stage, the thermalization distance is obtained as if the electron has 1.7 eV of kinetic energy, based on empirical data. The effect of different thermalization models available in Geant4-DNA has been described elsewhere [20].

The different parameters needed for the simulation of the physico-chemical and chemical stages of water radiolysis are gathered in a "chemistry constructor", which contains all information available for simulation of the water molecule dissociation scheme, definition of molecular species (including charge, mass, diffusion constant and van der Waals radius) and

chemical reactions they can undergo (including reaction rate coefficients). This constructor is named "G4EmDNAChemistry_option3" and is designed exclusively for this IRT approach, opposed to the other chemistry constructors available in Geant4-DNA, which are only used for the SBS approach. The list of available constructors dedicated to the chemical stage simulation are summarized in the table 1. The dissociation scheme of water molecules, following physical ionizations or electronic excitations, and corresponding branching ratios implemented in this constructor, from [20], are presented in the appendix (Table A1). In this constructor, for a complete simulation of water radiolysis, 15 molecular species listed in Table A2 are available (instead of 7 for the SBS constructors [43]). In addition, the 72 chemical reactions listed in tables A3–A7 are available (instead of 9 for the step-by-step constructors [44,45]).

2.2.2 Computational efficiency.—The computational efficiency ε, is a figure-of-merit that relates the computation time T spent to achieve a statistical variance, σ^2:

$$\varepsilon = \left(T\sigma^2\right)^{-1}.$$

(9)

In this work, ε was used to compare the computational efficiency of SBS and our IRT methods for the calculation of radiolytic yields, both implemented in Geant4-DNA as explained above. Simulations using both methods were performed to reach the same σ^2 for G-value calculations. We assume this can be achieved by simulating the same number of histories and using the same processes to model the physical (particle tracks) and pre-chemical (radiolysis) stages. The computational efficiency enhancement of the IRT over the SBS method was quantified by the reduced ratio ε_R, defined as the ratio between the computation times to simulate only the chemical stages, T_{SBS} and T_{IRT} with $\sigma^2_{SBS} = \sigma^2_{IRT}$, calculated as follows:

$$\varepsilon_R = T_{SBS}T_{IRT}^{-1}$$

(10)

The quantity ε_R is reported as a function of the unrestricted linear energy transfer (LET), averaged over simulated short track segments of electrons, protons or alpha particles. LET was calculated as the accumulated energy deposited in the scoring region, including all secondary electrons, divided by the primary track length [46]. For electrons, the simulation consisted of short track segments of initially monoenergetic electrons positioned at the center of a water cube of 1 cm side. The transport of each primary electron was terminated immediately after its accumulated energy loss exceeds a specific energy cut. Secondary electrons produced by inelastic interactions were transported down to the lower energy cut of Geant4-DNA model limits, see section 2.2.1. That criteria and energy cut values are given elsewhere [20,45]. For protons and alpha particles, short tracks segments were generated by terminating the transport of the primary particle at a pre-defined length. For protons, the track lengths ranged from 2.5 μm for the lowest energy value (0.5 MeV) to 20 μm for the highest energy value (100 MeV). For alpha particles, a 2.5 μm length was used for all the energy values (1 MeV/u to 12.5 MeV/u). The secondary electrons were simulated down to the energy limits of the Geant4-DNA's ELSEPA model for elastic scattering at 7.4 eV,
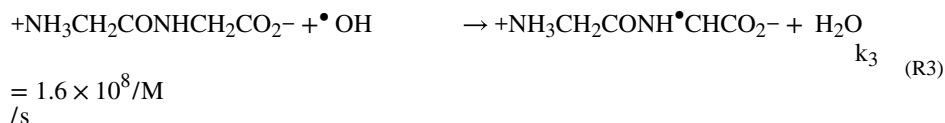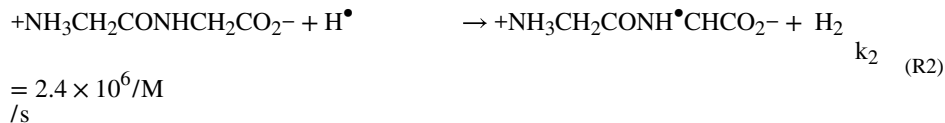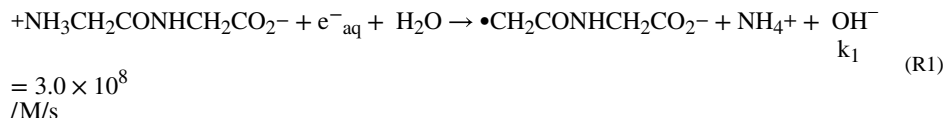
section 2.2.1 and [39]. Reference simulations, in terms of computational efficiency, were performed using the SBS method. For both IRT and SBS methods, 24 statistically independent simulations were run using the same CPU unit and the same number of primary histories, which ranged from 5 to 600 per simulation job for the highest-LET (alpha 4 MeV/u) and lowest-LET (electrons 1 MeV), respectively. Finally, ε_R was calculated using equation 9 and reported as the mean with its statistical uncertainty at one standard deviation. In all the simulations, the statistical uncertainty of the chemical yields was better than 0.5%, one standard deviation.

2.2.3   Time-dependent and LET-dependent G-values.—The set of reactions used are listed in the Appendix section; see also section 2.1.1. Simulations performed to compare SBS with IRT used only those reactions available in SBS, as marked in the appendix section. The branching ratios for the dissociation of water molecules and electron attachment are described in section 2.2.1. The simulation setups are described in section 2.2.2.

The time evolution of chemical yields was calculated using the first 10 keV of energy loss from 1 MeV electron tracks, which is a conventional method to perform G-values calculation for fast electrons [20,45–47]. At the sub nanosecond scale, calculated results were presented along with direct measurements of G-values in water for $^\bullet OH$ and e^-_{aq} from electron beams obtained with picosecond pulse radiolysis reported by [48][49][50] and [51]. At the microsecond scale, G-values were calculated for comparison to those measured for electron beams from Muroya et al [49] and ^{60}Co irradiation from LaVerne [52] and Yoshida et al. [53]

For LET-dependent yields, G-values at 1 μs were calculated for comparison to compiled experimental data. In most of the experimental LET data, measurements were obtained in the presence of scavengers, while the calculations were performed in pure water. A suitable comparison requires reproducing the experimental conditions in the simulation as best as possible, for example, simulating the same scavenger system used in each experiment. The objective of this work was to verify the reproducibility of the behavior of the chemical yields as the ionization density increases.

2.2.4   G-value calculation in the presence of scavengers.—The capability of the IRT implementation to model the presence of scavengers was verified for 1 MeV electrons (first 10 keV of energy deposited) and 2 MeV protons. The feature to simulate scavengers with the Geant4-DNA SBS was not available at this point. Simulations of the system containing glycylglycine at concentrations ranging from 10^{-4} M to 1 M (1 M = 1 mol dm^{-3}) were performed by adding the set of reactions (R1–R3). The bulk medium was made of liquid water ($\rho = 1$ g cm^{-3}) at neutral pH and ambient temperature. The yield of produced ammonium cation NH_4^+ from the scavenging of e^-_{aq} was calculated at the end of the chemical stage and compared with experimental values for a range of scavenger capacities from Yoshida et at. [53] for γ-rays and from LaVerne [54] for protons.

$$+NH_3CH_2CONHCH_2CO_2^- + e^-_{aq} + H_2O \rightarrow \bullet CH_2CONHCH_2CO_2^- + NH_4^+ + OH^-$$

$$= 3.0 \times 10^8 \text{ /M/s}$$

k_1 (R1)

$$+NH_3CH_2CONHCH_2CO_2^- + H^\bullet \rightarrow +NH_3CH_2CONH^\bullet CHCO_2^- + H_2$$

$$= 2.4 \times 10^6 \text{/M/s}$$

k_2 (R2)

$$+NH_3CH_2CONHCH_2CO_2^- + {}^\bullet OH \rightarrow +NH_3CH_2CONH^\bullet CHCO_2^- + H_2O$$

$$= 1.6 \times 10^8 \text{/M/s}$$

k_3 (R3)

3 Results.

3.1 Computational efficiency.

In Figure 4, ε_R is shown as a function of LET for simulations with the IRT method implemented in Geant4-DNA, calculated as the ratio of time taken in the chemistry portion of the simulation using SBS and IRT for the same calculation precision (Equation 9). A substantial efficiency improvement of three orders of magnitude was achieved with the IRT method implemented in Geant4-DNA for the lower LET electron and proton simulations. As the LET increases for the electron source, ε_R is reduced to a still significant factor of two.

3.2 Time-dependent and LET-dependent G-value.

Time-dependent G-values.—Figure 5 shows the time-dependent yields for the first 10 keV of energy deposited along 1 MeV electron tracks. From the graph on the left of the figure, it is shown that the material balance equation for oxidizing ($^\bullet$OH and H_2O_2) and reducing (e^-_{aq}, $H^\bullet$ and H_2) species is (almost) fulfilled with a statistically significant systematic deviation of 0.3% for both IRT and SBS implementations.

Figure 5 also shows the time-dependent G-value for $^\bullet$OH radical and e^-_{aq}. At the shorter times, IRT and SBS calculations agreed within combined statistical uncertainties, as the same physics models and pre-chemical dissociative channels were used. At longer times, IRT differed from SBS by up to −3.8% ± 0.1%, and −3.9% ± 0.1% for $^\bullet$OH and e^-_{aq}, respectively.

For $^\bullet$OH, direct measurements from irradiations of electrons in pure water for the shorter time range (< 10 ns) from El Omar et al. [50] and Wang et al. [51] are shown. The magnitude of the experimental error is shown at a single time of 10^{-2} ns for clarity. The obtained decay of $^\bullet$OH yields from 7×10^{-3} ns to 8 ns for both IRT and SBS methods exceed the more recent experimental yields from Wang et al. [51] at 7×10^{-3} ns by 0.3 ± 0.12 molec./100 eV, one

standard deviation. At 10^3 ns, IRT and SBS exceed the experimental data by 0.22 ± 0.12 molec./100 eV and 0.32 ± 0.12 molec./100 eV, one standard deviation, respectively.

For solvated electrons, at the earliest times both IRT and SBS calculations agreed with direct measurements from Bartels et al[48], El Omar et al[50] and Wang et al[51], within one standard deviation of the experimental error. At longer times, calculated data from both methods agreed with the experimental data from Yoshida et al [53] within one standard deviation.

LET-dependent G-values.—Figure 6 shows the LET-dependent G-value for electrons, protons and alpha particles calculated with IRT and SBS. The material balance equation, represented as the ratio between oxidative to reduced species as a function of the LET, is shown in the bottom right of Figure 6. The ratio reaches unity within statistical uncertainties for protons and alpha particles, but deviates from unity by 0.3% for electrons, as seen in Figure 6. Measured data from the literature are also displayed from different particles. For the chemical species displayed in Figure 6, the calculated yields reproduce the change in the experimental data as the LET increases. That is, although the yield of $H^{\bullet}$ and H_2O_2 are significantly higher in the simulation than the experiments, the slope of the yield with LET is in reasonable agreement.

G-value calculation in the presence of scavengers.—Modeling the presence of scavengers is shown in Figure 7 for the yield of NH_4^+ produced by electrons and protons as a function of the scavenging capacity. For electrons, calculated data from LaVerne et al [54] using IRT is also shown. The experimental data from cobalt-60 γ-rays irradiation, which result in a scavenging capacity comparable to electrons, is from Yoshida et al [53]. As shown, a consistent agreement of the behavior of NH_4^+ yields is fairly reproduced by the Geant4-DNA implementation of IRT. For low energy protons, measured data are reported as track-averaged G-values while the IRT calculation is typically calculated with track-segment G-value, which is calculated over an almost constant LET across a short track-segment. The comparison of both track-segment and track-averaged G-values are shown in Figure 7. The track-averaged G-values were obtained by integrating the G-values from short proton track-segments from 2 MeV to 0.1 MeV, the limit of the Geant4-DNA models for protons. Results are consistent with calculated data from LaVerne et al [54] where the G-values are also reported as a track-averaged quantity.

4 Discussion.

In this work, an implementation of the independent reaction times (IRT) in Geant4-DNA was presented. A substantial improvement in the computational efficiency was achieved, up to three orders of magnitude at low LET, decreasing as the particle LET increases. This decrease was caused by the increase in the density of ionized and excited events from high LET particles compared to low LET particles. As a consequence, the increased number of neighbor initial chemical species looked by the IRT searching algorithm, as implemented, demanded more operations as the complexity of this algorithm is O(N(N-1)/2). Thus, degrading in the efficiency with increasing the LET was expected. Implementing a neighbor searching algorithm, for example, by adopting the kd-tree algorithm available in Geant4-

DNA[19], and the implementation of a cutoff distance [25] as a function of the LET, will potentially mitigate such reduction in efficiency.

A systematic deviation of 0.3% from unity was found for the ratio between oxidative species to reduced species for electron tracks calculated with both SBS and IRT. The difference might be caused by the lack of dissociation scheme of the double ionized water molecules induced by Auger electrons produced by our implementation of the physics list, but are currently considered as single ionized water molecules in our simulation. However, this discrepancy is well below the experimental uncertainty of 5% typically reported, shown in the center and right panels of Figure 5, and is thus results in a negligible systematic error.

For time-dependent G-values a clear difference was found between IRT and SBS at longer times, hence, also reflected in LET-dependent G-values. The differences might be attributed in part to the independent pair approximation taken by the IRT approach whereas the SBS considers a multiparticle system [55]. Nevertheless, it has been shown that the yields calculated with SBS are equivalent to IRT when using two-particle systems [3,24,56]. In addition, the G-values calculated with the SBS approach depended to some extent on the minimum time step which is implemented in a dynamic time partition[19]. To quantify this effect, we calculated G-values for $^{\bullet}$OH produced by 1 MeV electrons using a fixed minimum time step to 0.1 ps. While the G-value for solvated electrons remained unaffected, our results showed that the G-value for $^{\bullet}$OH reduced by 2.6% at 1 μs when the fixed minimum time step was used instead of the default values used by the dynamic time step (see table 4 in Karamitros et al [18]). However, we kept the latter time step configuration in all the simulations because the systematic difference, smaller than reported experimental errors, was tolerated given the computational overhead of four-fold introduced by the use of a small-time step.

A significant overestimate of G-values, outside the experimental error of the latest $^{\bullet}$OH measurements from Wang et al [51], was found for both SBS and IRT at 10^{-2} ns. The data from Wang et al is the most recent data obtained at the shortest time following irradiation (7 ps). To resolve this mismatch, a comprehensive revision of the current physical and water dissociative schemes implemented in Geant4-DNA, following Wang et al [51] data, is encouraged. That revision task is an ongoing work within our group that began with the revision of the physical models as reported recently[20]. We expect that the revision of physical and pre-chemical processes also has a good impact in the Geant4-DNA accuracy at the steady state (10^3 ns), where currently a reasonable agreement is found. Nevertheless, for e^-_{aq} a satisfactory agreement was found within the experimental error over the entire time domain.

The evolution of G-values as a function of the particle LET were reproduced by both SBS and IRT. The magnitude of the calculated yields was in reasonable agreement with measured data for most of the species, considering the experimental uncertainties, and considering that the measurements were performed in the presence of scavengers, while calculations were performed in pure liquid water. A strict comparison between calculated and measured data requires strict adherence to the experimental conditions in the simulations, including the presence of scavengers, the comparison of track-averaged and track-segment G-values

(Figure 5), and the implementation of the multiple ionization process, shown to improve the accuracy for H_2O_2 in the high LET range [28,57].

5   Conclusions.

In this work, the Independent Reaction Times method that simulates the reaction kinetics following the interaction of ionizing radiation was successfully implemented in Geant4-DNA. The implementation achieves a substantial computational efficiency over the existing step-by-step method (SBS) of Geant4-DNA by up to three orders of magnitude. Both methods achieve similar accuracy when compared to experimental data of time-dependent and LET-dependent G-values. The lack of consideration of partially diffusion-controlled reactions in the SBS with the selection of a dynamic time step resolution causes a difference in G-values by 3.9% with respect to IRT data at 1 μs. The capabilities of simulating systems with scavengers was demonstrated and showed satisfactory agreement with experimental data. However, for $^{\bullet}OH$ radical yields, there was a significant overestimate of 5% at the earliest time (7 ps) from recently measured yields. Further work to resolve such differences is ongoing within our group. The implementation presented here is a step forward to facilitate such studies.

Supplementary Material

Refer to Web version on PubMed Central for supplementary material.

Acknowledgments.

Appendix A

The dissociation schemes, list of chemical species and list of reactions available in the Geant4-DNA IRT implementation are shown in Tables A1, A2 and A3 to A7, respectively. The classification of reactions is that proposed by Frongillo et al [5]. The reaction rate coefficients are from Plante and Devroye [3]. The molar concentration M is equal to 1 mol dm^{-3}

References.

1. Nikjoo H, Emfietzoglou D, Liamsuwan T, Taleei R, Liljequist D, Uehara S. Radiation track, DNA damage and response—a review. Reports Prog Phys. 2016;79(11):116601. doi:10.1088/0034-4885/79/11/116601

2. Dingfelder M, Hantke D, Inokuti M, Paretzke HG. Electron inelastic-scattering cross sections in liquid water. Radiat Phys Chem. 1999;53(1):1–18. doi:10.1016/S0969-806X(97)00317-4

3. Plante I, Devroye L. Considerations for the independent reaction times and step-by-step methods for radiation chemistry simulations. Radiat Phys Chem. 2017;139(September 2016):157–172. doi:10.1016/j.radphyschem.2017.03.021

4. Boscolo D, Krämer M, Durante M, Fuss MC, Scifoni E. TRAX-CHEM: A pre-chemical and chemical stage extension of the particle track structure code TRAX in water targets. Chem Phys Lett. 2018;698:11–18. doi:10.1016/j.cplett.2018.02.051

5. Frongillo Y, Goulet T, Fraser M-J, Cobut V, Patau JP, Jay-Gerin J-P. Monte Carlo Simulation of Fast Electron And Proton Tracks In Liquid Water - II. Nonhomogeneous Chemistry. Radiat Phys Chem. 1998;51(3):245–254. doi:10.1016/S0969-806X(97)00097-2

6. Incerti S, Baldacchino G, Bernal M, et al. THE Geant4-DNA project. Int J Model Simulation, Sci Comput. 2010;1(2):157–178. doi:10.1142/S1793962310000122

7. Incerti S, Ivanchenko A, Karamitros M, et al. Comparison of GEANT4 very low energy cross section models with experimental data in water. Med Phys. 2010;37(9):4692–4708. doi:10.1118/1.3476457 [PubMed: 20964188]

8. Bernal MA, Bordage MC, Brown JMC, et al. Track structure modeling in liquid water: A review of the Geant4-DNA very low energy extension of the Geant4 Monte Carlo simulation toolkit. Phys Med. 2015;31(8):861–874. doi:10.1016/j.ejmp.2015.10.087 [PubMed: 26653251]

9. Incerti S, Kyriakou I, Bernal MA, et al. Geant4-DNA example applications for track structure simulations in liquid water: A report from the Geant4-DNA Project. Med Phys. 2018;45(8):e722–e739. doi:10.1002/mp.13048

10. Friedland W, Schmitt E, Kundrát P, et al. Comprehensive track-structure based evaluation of DNA damage by light ions from radiotherapy-relevant energies down to stopping. Sci Rep. 2017;7(March):45161. doi:10.1038/srep45161 [PubMed: 28345622]

11. Lampe N, Karamitros M, Breton V, et al. Mechanistic DNA damage simulations in Geant4-DNA Part 2: Electron and proton damage in a bacterial cell. Phys Medica. 2018;48(June 2017):146–155. doi:10.1016/j.ejmp.2017.12.008

12. Sakata D, Lampe N, Karamitros M, et al. Evaluation of early radiation DNA damage in a fractal cell nucleus model using Geant4-DNA. Phys Medica. 2019;62(January):152–157. doi:10.1016/j.ejmp.2019.04.010

13. Meylan S, Incerti S, Karamitros M, et al. Simulation of early DNA damage after the irradiation of a fibroblast cell nucleus using Geant4-DNA. Sci Rep. 2017;7(1):1–15. doi:10.1038/s41598-017-11851-4 [PubMed: 28127051]

14. Tang N, Bueno M, Meylan S, et al. Influence of chromatin compaction on simulated early radiation-induced DNA damage using Geant4-DNA. Med Phys. 2019;46(3):1501–1511. doi:10.1002/mp.13405 [PubMed: 30689203]

15. Agostinelli S, Allison J, Amako K, et al. GEANT4 - A simulation toolkit. Nucl Instruments Methods Phys Res Sect A Accel Spectrometers, Detect Assoc Equip. 2003;506(3):250–303. doi:10.1016/S0168-9002(03)01368-8

16. Allison J, Amako K, Apostolakis J, et al. Geant4 developments and applications. IEEE Trans Nucl Sci. 2006;53(1):270–278. doi:10.1109/TNS.2006.869826

17. Allison J, Amako K, Apostolakis J, et al. Recent developments in GEANT4. Nucl Instruments Methods Phys Res Sect A Accel Spectrometers, Detect Assoc Equip. 2016;835:186–225. doi:10.1016/j.nima.2016.06.125

18. Karamitros M, Mantero A, Incerti S, et al. Modeling Radiation Chemistry in the Geant4 Toolkit. Prog Nucl Sci Technol. 2011;2:503–508. http://www.aesj.or.jp/publication/pnst002/data/503-508.pdf.

19. Karamitros M, Luan S, Bernal MA, et al. Diffusion-controlled reactions modeling in Geant4-DNA. J Comput Phys. 2014;274:841–882. doi:10.1016/j.jcp.2014.06.011

20. Shin W-G, Ramos-Mendez J, Faddegon B, et al. Evaluation of the influence of physical and chemical parameters on water radiolysis simulations under MeV electron irradiation using Geant4-DNA. J Appl Phys. 2019;126(11):114301. doi:10.1063/1.5107511

21. Schuemann J, McNamara AL, Ramos-Méndez J, et al. TOPAS-nBio: An Extension to the TOPAS Simulation Toolkit for Cellular and Sub-cellular Radiobiology. Radiat Res. 2018;191(2):125. doi:10.1667/RR15226.1

22. Ramos-Méndez J, Burigo LN, Schulte R, Chuang C, Faddegon B. Fast calculation of nanodosimetric quantities in treatment planning of proton and ion therapy. Phys Med Biol. 2018;63(23):235015. doi:10.1088/1361-6560/aaeeee [PubMed: 30484432]

23. Ivanchenko V, Apostolakis J, Bagulya a., et al. Recent Improvements in Geant4 Electromagnetic Physics Models and Interfaces. 3th Monte Carlo Conf MC 2010. 2011;2:898–903. http://hal.in2p3.fr/in2p3-00658779.

24. Clifford P, Green NJB, Oldfield MJ, Pilling MJ, Pimblott SM. Stochastic Models of Multi-species Kinetics in Radiation-induced Spurs. J Chem Soc, Faraday Trans 1. 1986;82:2673–2689. doi:10.1039/F19868202673

25. Green NJB, Pilling MJ, Clifford P. Stochastic Modeling of Fast Kinetics in a Radiation Track. Society. 1990;94(1):251–258. doi:10.1021/j100364a041

26. Pimblott SM, Pilling MJ, Green NJB. Stochastic models of spur kinetics in water. Int J Radiat Appl Instrumentation Part. 1991;37(3):377–388. doi:10.1016/1359-0197(91)90006-N

27. Tomita H, Kai M, Kusama T, Ito A. Monte Carlo simulation of physicochemical processes of liquid water radiolysis. Radiat Environ Biophys. 1997;36(2):105–116. doi:10.1007/s004110050061 [PubMed: 9271798]

28. Gervais B, Beuve M, Olivera GH, Galassi ME. Numerical simulation of multiple ionization and high LET effects in liquid water radiolysis. Radiat Phys Chem. 2006;75(4):493–513. doi:10.1016/j.radphyschem.2005.09.015

29. Tomita H, Kai M, Kusama T, Ito A. Monte Carlo simulation of DNA strand-break induction in supercoiled plasmid pBR322 DNA from indirect effects. Radiat Environ Biophys. 1998;36(4):235–241. doi:10.1007/s004110050077 [PubMed: 9523339]

30. Karamitros M, Brown J, Lampe N, et al. Implementing the Independent Reaction Time method in Geant4 for radiation chemistry simulations. 2020.

31. Sanguanmith S, Meesungnoen J, Muroya Y, Lin M, Katsumura Y, Jay-Gerin JP. On the spur lifetime and its temperature dependence in the low linear energy transfer radiolysis of water. Phys Chem Chem Phys. 2012;14(48):16731–16736. doi:10.1039/c2cp42826a [PubMed: 23138332]

32. Sano H, Tachiya M. Partially diffusion-controlled recombination. J Chem Phys. 1979;71(3):1276–1282. doi:10.1063/1.438427

33. Tachiya M Theory of diffusion-controlled reactions: Formulation of the bulk reaction rate in terms of the pair probability. Radiat Phys Chem. 1983;21(1–2):167–175. doi:10.1016/0146-5724(83)90143-7

34. Agostinelli S, Allison J, Amako K, et al. Geant4—a simulation toolkit. Nucl Instruments Methods Phys Res Sect A Accel Spectrometers, Detect Assoc Equip. 2003;506(3):250–303. doi:10.1016/S0168-9002(03)01368-8

35. Goulet T, Jay-Gerin JP. On the reactions of hydrated electrons with OH. and H 3O+. Analysis of photoionization experiments. J Chem Phys. 1992;96(7):5076–5087. doi:10.1063/1.462751

36. Lazarakis P, Incerti S, Ivanchenko V, et al. Investigation of track structure and condensed history physics models for applications in radiation dosimetry on a micro and nano scale in Geant4. Biomed Phys Eng Express. 2018;4(2):024001. doi:10.1088/2057-1976/aaa6aa

37. Emfietzoglou D Inelastic cross-sections for electron transport in liquid water: A comparison of dielectric models. Radiat Phys Chem. 2003;66(6):373–385. doi:10.1016/S0969-806X(02)00504-2

38. Rudd ME, Kim Y-K, Märk T, Schou J, Stolterfoht N, Toburen LH. ICRU Report 55. J Int Comm Radiat Units Meas. 1996;os28(2):NP–NP. doi:10.1093/jicru/os28.2.Report55

39. Shin WG, Bordage MC, Emfietzoglou D, et al. Development of a new Geant4-DNA electron elastic scattering model for liquid-phase water using the ELSEPA code. J Appl Phys. 2018;124(22). doi:10.1063/1.5047751

40. Bote D, Salvat F, Jablonski A, Powell CJ. The effect of inelastic absorption on the elastic scattering of electrons and positrons in amorphous solids. J Electron Spectros Relat Phenomena. 2009;175(1–3):41–54. doi:10.1016/j.elspec.2009.07.003

41. Michaud M, Wen A, Sanche L. Cross Sections for Low-Energy (1–100 eV) Electron Elastic and Inelastic Scattering in Amorphous Ice. Radiat Res. 2003;159(1):3–22. doi:10.1667/0033-7587(2003)159[0003:csflee]2.0.co;2 [PubMed: 12492364]

42. Meesungnoen J, Jay-Gerin J-P, Filali-Mouhim A, Mankhetkorn S. Low-Energy Electron Penetration Range in Liquid Water. Radiat Res. 2002;158(5):657–660. doi:10.1667/0033-7587(2002)158[0657:leepri]2.0.co;2 [PubMed: 12385644]

43. Peukert D, Incerti S, Kempson I, et al. Validation and investigation of reactive species yields of Geant4-DNA chemistry models. Med Phys. 2019;46(2):983–998. doi:10.1002/mp.13332 [PubMed: 30536689]

44. Kreipl MS, Friedland W, Paretzke HG. Time- and space-resolved Monte Carlo study of water radiolysis for photon, electron and ion irradiation. Radiat Environ Biophys. 2009;48(1):11–20. doi:10.1007/s00411-008-0194-8 [PubMed: 18949480]

45. Ramos-Méndez J, Perl J, Schuemann J, McNamara A, Paganetti H, Faddegon B. Monte Carlo simulation of chemistry following radiolysis with TOPAS-nBio. Phys Med Biol. 2018;63(10):105014. doi:10.1088/1361-6560/aac04c [PubMed: 29697057]

46. Uehara S, Nikjoo H. Monte Carlo simulation of water radiolysis for low-energy charged particles. J Radiat Res. 2006;47(1):69–81. doi:10.1269/jrr.47.69 [PubMed: 16571920]

47. Pimblott SM, LaVerne JA. Stochastic Simulation of the Electron Radiolysis of Water and Aqueous Solutions. J Phys Chem A. 1997;101(33):5828–5838. doi:10.1021/jp970637d

48. Bartels DM, Cook AR, Mudaliar M, Jonah CD. Spur decay of the solvated electron in picosecond radiolysis measured with time-correlated absorption spectroscopy. J Phys Chem A. 2000;104(8):1686–1691. doi:10.1021/jp992723e

49. Muroya Y, Lin M, Wu G, et al. A re-evaluation of the initial yield of the hydrated electron in the picosecond time range. Radiat Phys Chem. 2005;72(2–3):169–172. doi:10.1016/j.radphyschem.2004.09.011

50. El Omar AK, Schmidhammer U, Jeunesse P, et al. Time-dependent radiolytic yield of OH• radical studied by picosecond pulse radiolysis. J Phys Chem A. 2011;115(44):12212–12216. doi:10.1021/jp208075v [PubMed: 21970432]

51. Wang F, Schmidhammer U, Larbre JP, Zong Z, Marignier JL, Mostafavi M. Time-dependent yield of the hydrated electron and the hydroxyl radical in D2O: A picosecond pulse radiolysis study. Phys Chem Chem Phys. 2018;20(23):15671–15679. doi:10.1039/c8cp02276c [PubMed: 29845125]

52. Laverne JA. OH Radicals and Oxidizing Products in the Gamma Radiolysis of Water. Source Radiat Res Radiat Res Gamma Radiolysis Water Radiat Res. 2000;(153):53–196. http://www.jstor.org/stable/3580071 Accessed February 15, 2017.

53. Yoshida H, Bolch WE, Jacobson KB, Turner JE. Measurement of free ammonia produced by X irradiation of glycylglycine in aqueous solution. Radiat Res. 1990;121(3):257–261. doi:10.2307/3577774 [PubMed: 2315444]

54. LaVerne JA, Štefani I, Pimblott SM. Hydrated Electron Yields in the Heavy Ion Radiolysis of Water. J Phys Chem A. 2005;109(42):9393–9401. doi:10.1021/jp0530303 [PubMed: 16866387]

55. Al-Samra EH, Green NJB. On the approximation of independent pairs in diffusion kinetics: Correlation of distances in a three-body system. Phys Chem Chem Phys. 2018;20(4):2872–2879. doi:10.1039/c7cp06929d [PubMed: 29327022]

56. Pimblott SM, Green NJB. Stochastic modeling of partially diffusion-controlled reactions in spur kinetics. J Phys Chem. 1992;96(23):9338–9348. doi:10.1021/j100202a052

57. Meesungnoen J, Jay-Gerin J-P. Effect of multiple ionization on the yield of H2O2 produced in the radiolysis of aqueous 0.4 M H2SO4 solutions by high-LET 12C6+ and 20Ne9+ ions. Radiat Res. 2005;164(5):688–694. doi:10.1667/RR3459.1 [PubMed: 16238448]

58. Karamitros M Extension de l'outil Monte Carlo généraliste Geant4 pour la simulation de la radiolyse de l'eau dans le cadre du projet Geant4-DNA. 2013 https://www.dropbox.com/s/r4grkm83uprchcd/These_MKaramitros.pdf%5Cnpapers3://publication/uuid/6BC42EC2-1ECD-47CB-84EC-DECE3E1B2CD3.

59. Burns WG. Effect of Radiation Type in Water Radiolysis. J Chem SOC Faraday Trans I. 1981;77:2803–2813.

60. Appleby A, Schwarz HA. Radical and molecular yields in water irradiated by .gamma.-rays and heavy ions. J Phys Chem. 1969;73(6):1937–1941. doi:10.1021/j100726a048

61. Anderson AR, Hart EJ. Molecular Product and Free Radical Yields in the Decomposition of Water by Protons, Deuterons, and Helium Ions. Radiat Res. 1961;14(6):689–704. doi:10.2307/3571010 [PubMed: 13683173]

62. Sauer MC, Schmidt KH, Hart EJ, Naleway CA, Jonah CD. LET dependence of transient yields in the pulse radiolysis of aqueous systems with deuterons and alpha particles. Radiat Res. 1977;70(1):91–106. doi:10.2307/3574734 [PubMed: 850737]

63. Elliot A et al. Temperature Dependence of g Values for H2O and D2O irradiated with Low Linear Energy Transfer Radiation. J Chem Soc Faraday Trans. 1993;89(8):1193–1197. doi:10.1039/FT9938901193

64. Pastina B, LaVerne JA. Hydrogen Peroxide Production in the Radiolysis of Water with Heavy Ions. J Phys Chem A. 1999;103(11):1592–1597. doi:10.1021/jp984433o

65. Wasselin-Trupin V, Baldacchino G, Bouffard S, Hickel B. Hydrogen peroxide yields in water radiolysis by high-energy ion beams at constant LET. Radiat Phys Chem. 2002;65(1):53–61. doi:10.1016/S0969-806X(01)00682-X

66. Crumière F, Vandenborre J, Essehli R, Blain G, Barbet J, Fattahi M. LET effects on the hydrogen production induced by the radiolysis of pure water. Radiat Phys Chem. 2013;82(1):74–79. doi:10.1016/j.radphyschem.2012.07.010
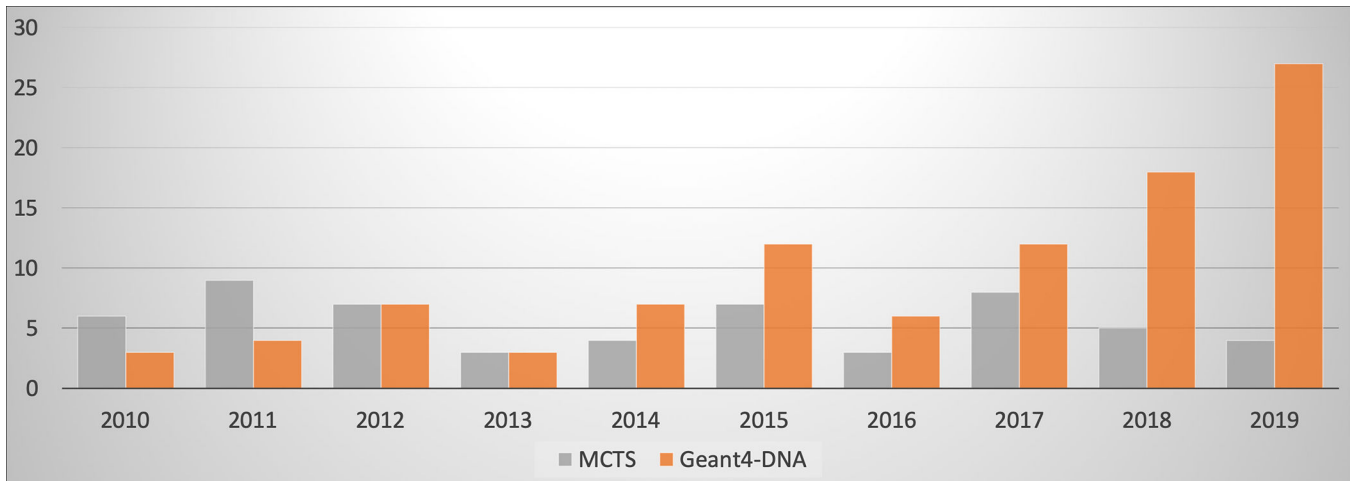
67. Stroustrup B The C ++ Programming; 1986.

Figure 1 :
Number of publications per year in biomedical science listed in PubMed. Search parameters: Geant4-DNA or Monte Carlo track-structure. Search criteria: appeared in the abstract of publications. Search date: February 10, 2020.
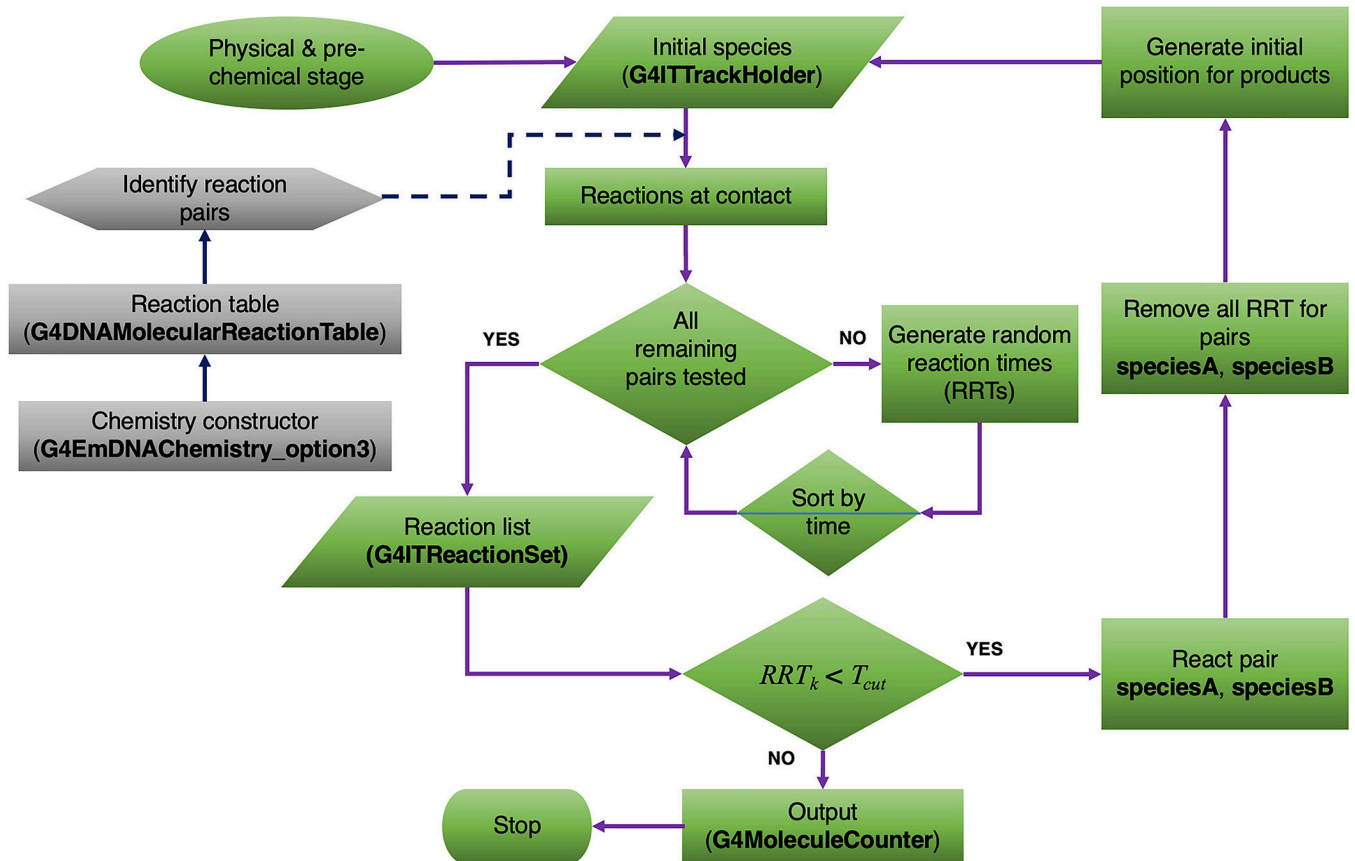
Figure 2 :
Flowchart of IRT implemented in Geant4-DNA (version 10.7 beta, June 2020).
G4ITTrackHolder, G4ITReactionSet, G4DNAMolecularReactionTable and
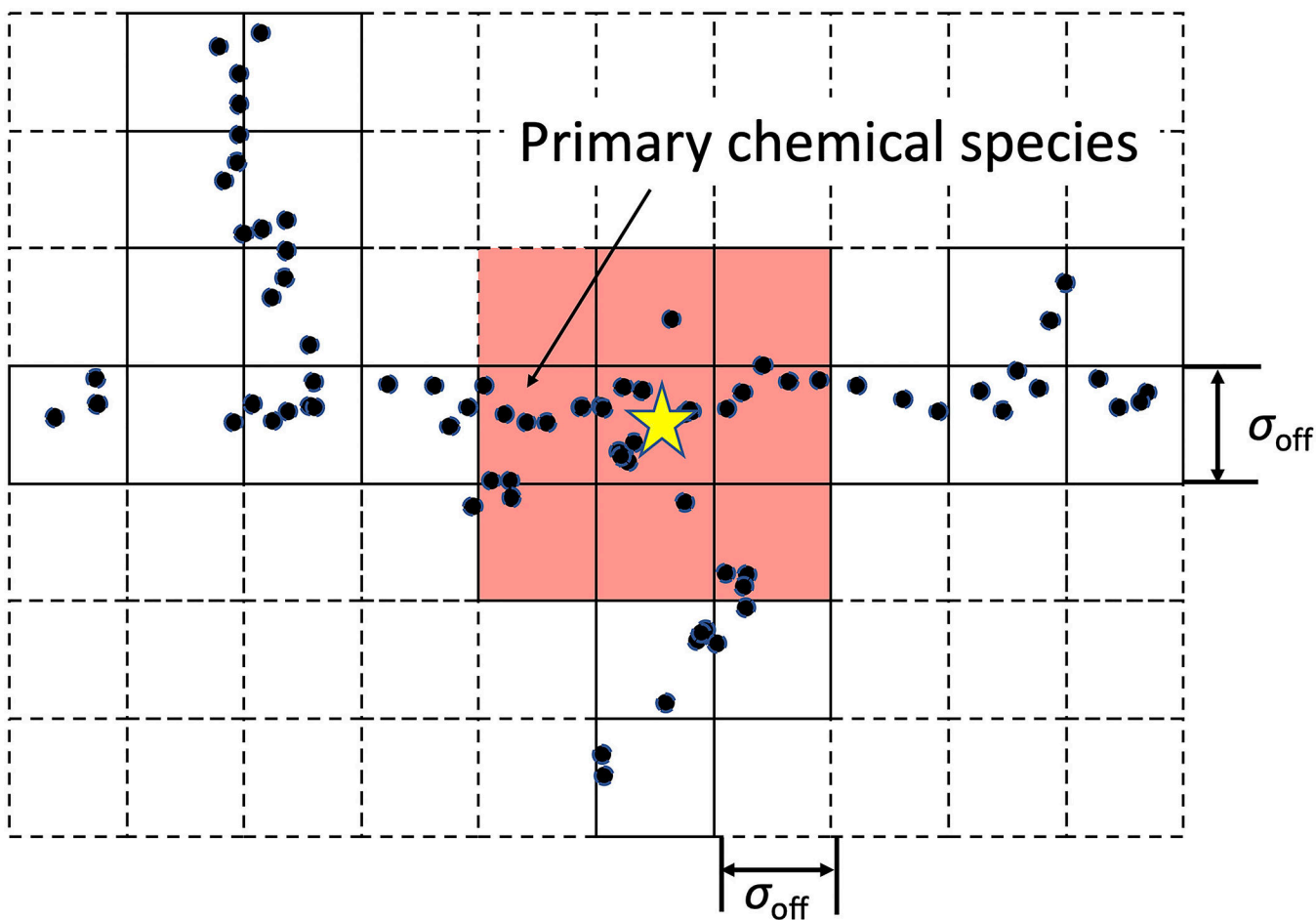G4MoleculeCounter classes are developments already available from the step-by-step
implementation [19], [58].

Figure 3 :

A schematic illustration of the voxelization of the chemical track into cubic voxels of side length σ_{off}. The black points represent chemical species at the end of the pre-chemical stage, the yellow star indicates a target molecule, and the red voxels represent scanned regions, searching for the target molecule.
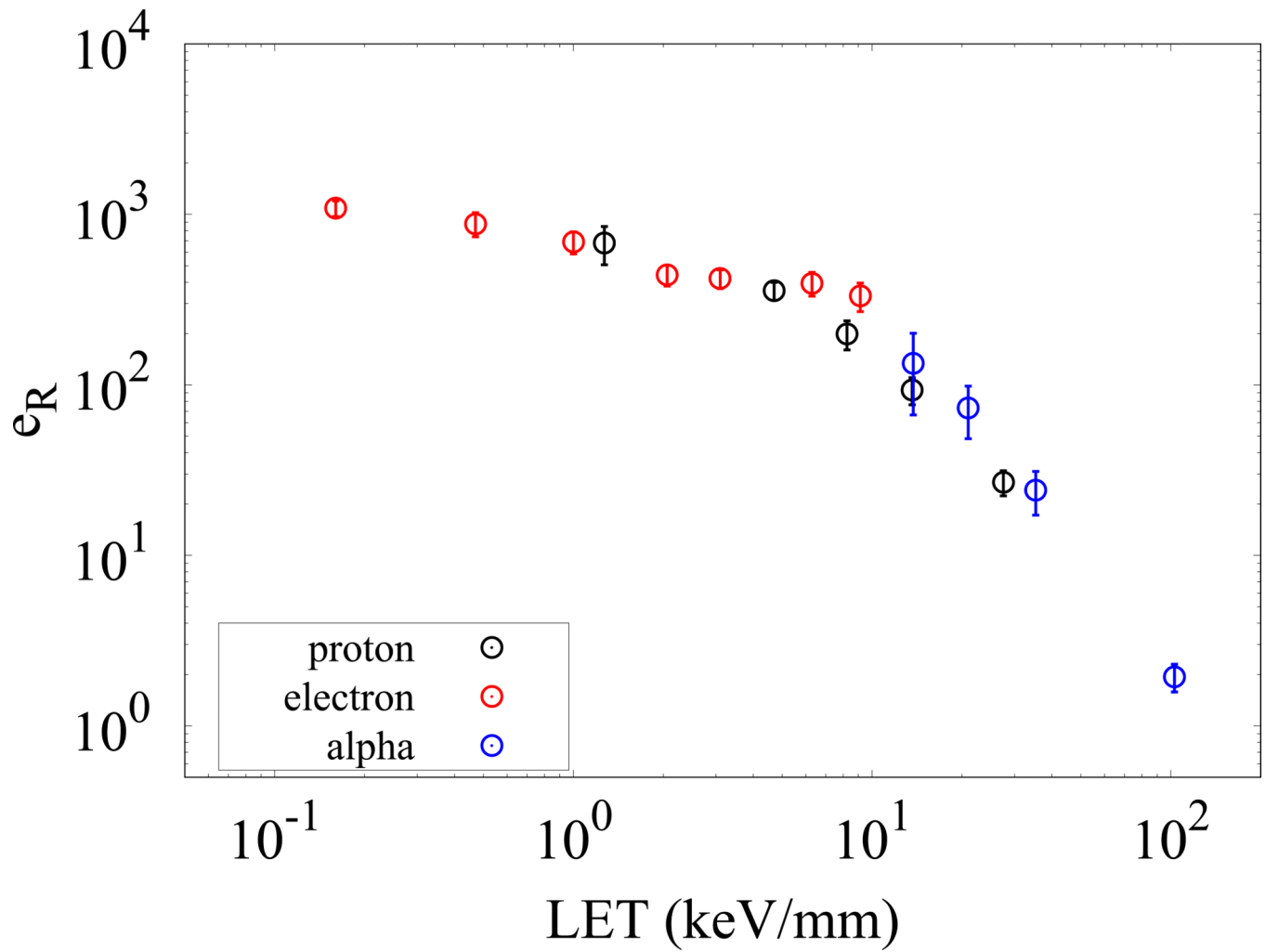
Figure 4:
LET-dependent computational efficiency of IRT implemented in Geant4-DNA relative to the
SBS method. Results are shown for electrons (red), protons (black) and alpha particles
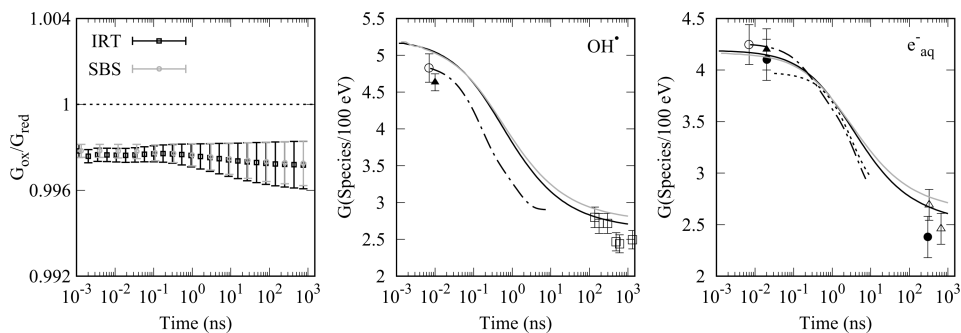(blue). Error bars represent one standard deviation of statistical uncertainty.

Figure 5:
Calculated time dependent ratio between oxidative and reductive G-Values from the first 10 keV energy deposited by 1 MeV electrons (left) from Geant4 IRT (black points) and SBS (light gray points). Error bars represent combined statistical uncertainty, one standard deviation. Time-depended G-values for $^\bullet$OH radical (center) and solvated electron (right) from IRT (black lines) and SBS (light gray lines). Experimental data from pulse radiolysis are shown at shorter times with filled triangles[50], empty circles and dotted-dashed lines [51], dot-dashed lines [48] (using a time correlation method) and filled circles [49]. At longer times, data from ^{60}Co irradiations are shown with empty squares[52], filled circles [49] and empty triangles[53]. Experimental errors represent one standard deviation.
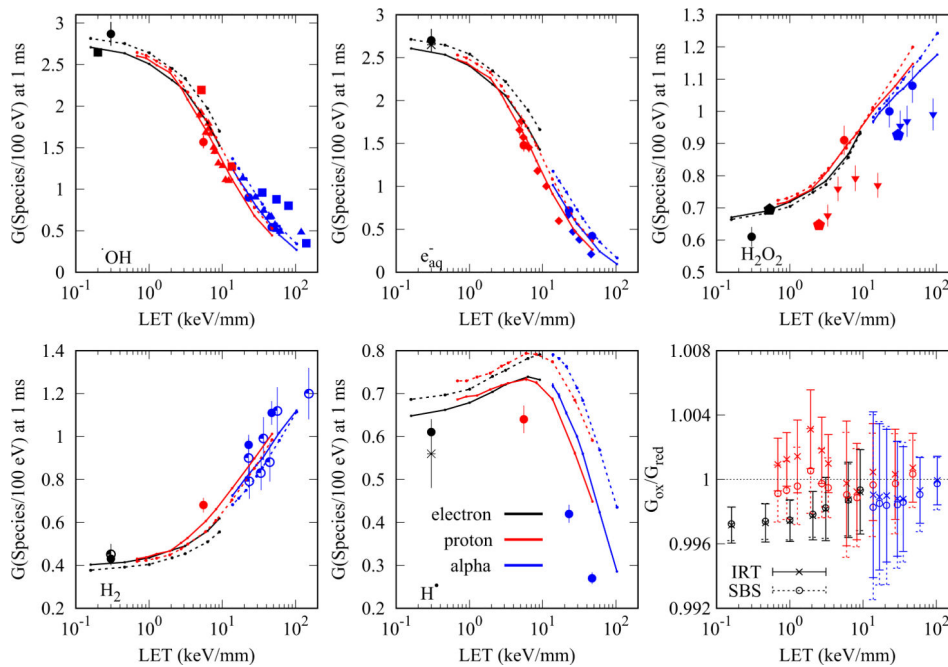
Figure 6:

Unrestricted LET-dependent G-values at 1 µs for electrons (black), protons (red) and alpha particles (blue). IRT calculations are shown with solid lines connecting crosses and SBS are shown with dotted lines connecting empty circles. Experimental data from γ-rays (black), proton or deuteron (red) and alpha particles (blue) are shown with symbols: filled square[59], filled circle[60], filled triangle[61], filled diamond[62], star[63], inverted triangle[64], filled polygon[65], and semi filled circle[66]. Experimental error bars represent one standard deviation. The LET-dependent ratio between oxidative and reduction species is shown at the bottom right panel. Error bars represent combined statistical uncertainty, one standard deviation.
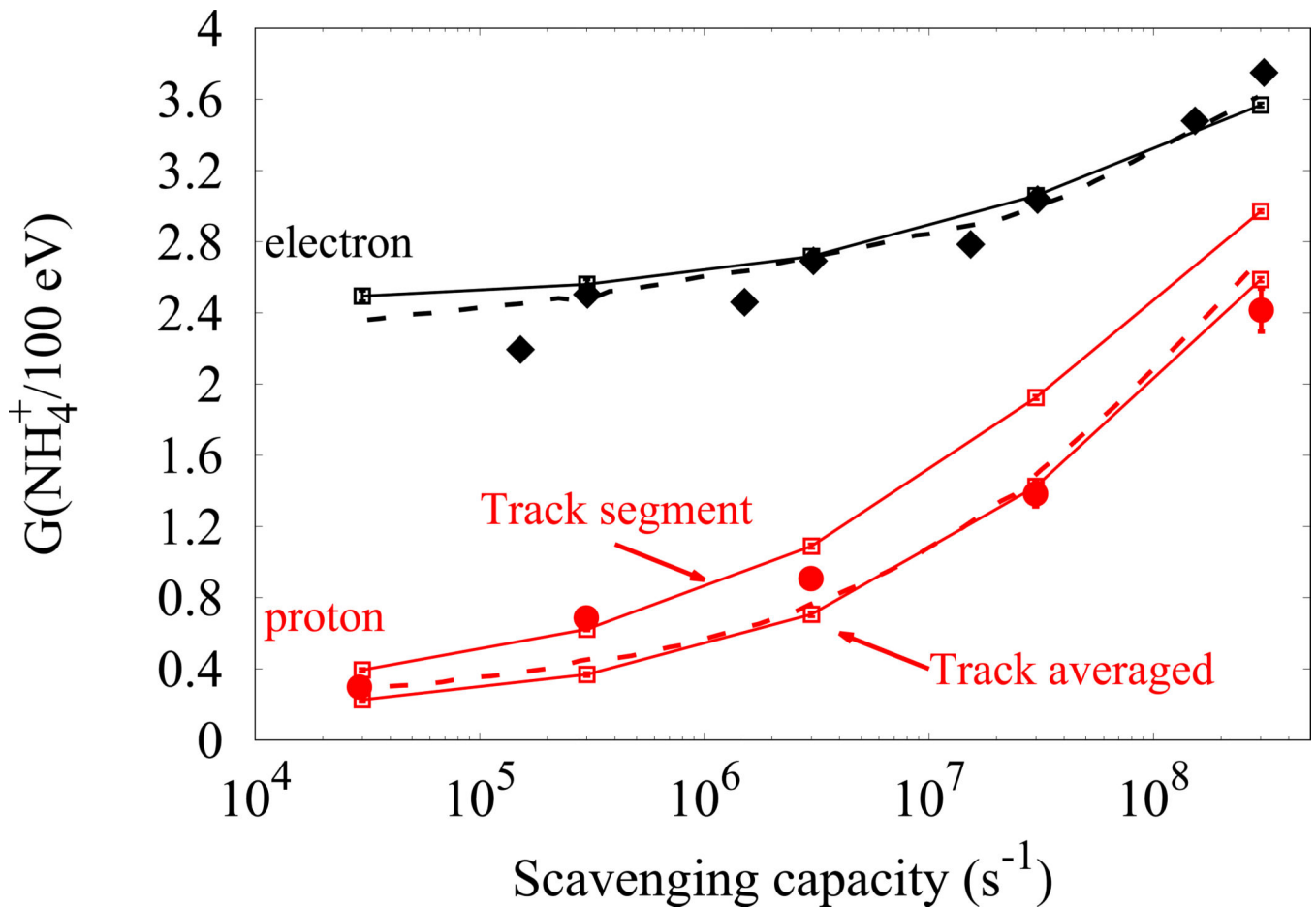
Figure 7 :

Calculated NH_4^+ yields with Geant4-DNA IRT (empty squares connected with solid lines) and from LaVerne [54] (dashed lines) at different scavenging capacities of glycylglycine. Electron irradiation (black) simulations are compared to measured data for cobalt-60 from Yoshida et al [53] (solid diamonds). Data for 2 MeV proton (red) simulations are compared to measured data from LaVerne [54] (filled circles.) For protons, both track-segment and track-averaged G-values are shown.

Table 1

Chemistry constructors available in Geant4-DNA.

Geant4-DNA Constructor	Description
G4EmDNAChemistry	First constructor implemented in Geant4-DNA for the chemistry processes with parameter values from Karamitros et al [18,19]
G4EmDNAChemistry_option1	Implements a revisited set of chemistry parameters used in Shin et al [20]
G4EmDNAChemistry_option2	Includes chemistry parameters for simulating reactions with DNA components.
G4EmDNAChemistry_option3	Implements the IRT approach presented in this work.